Non-Hermitian Optical Tunable System Based on Lithium Niobate Coupling Resonator

Xianpeng Lv, Qijing Lin, Wentao Qiu, Heyuan Guan, and Huihui Lu

***Abstract*—Recently, an exceptional point (EP) was constructed in a coupled double-ring resonator. Generally, such non-Hermitian optical systems are realized via material selection and a spatially precise layout. However, because of material limitations, some system parameters cannot be changed after the waveguide is fabricated. In this study, We demonstrate a lithium niobate-based tunable system for controlling system dispersion and loss, the resonator structure made of lithium niobate is theoretically and numerically investigated and analyzed. Lithium niobate is chosen because it exhibits good electro-optic properties. Furthermore, the real part of the potential energy term of the non-Hermitian system is regulated using external electric field. Consequently, a frequency shift of up to 149 GHz is observed in the double characteristic peak of the transmission spectrum with a contrast of up to 0.43. In addition, a gain-influenced EP is observed in a coupled dual-ring resonator system by introducing gain material. It has potential application in future optical fiber communication, optical quantum computing, and environmental sensing.**

***Index Terms*—Coupled resonators, electro-optical effects, integrated optics, optical waveguides.**

I. Introduction

THE Hermitian Hamiltonian theoretical system originates from a closed system in quantum mechanics. However, the open system with gain and loss can express more complex systems; In this regard, a non-Hermitian Hamiltonian theoretical system was established [1], [2], [3]. In an open system of quantum mechanics, for a system that contains loss and gain, the eigenvalue of the Hamiltonian operator has a complex form. In 1998, Bender et al. [3]. proved that the PT-symmetric non-Hermitian Hamiltonian has real eigenvalues. With the maturation of integrated optical technology, a PT-symmetric system on an optical platform has been realized and investigated in this regard. In particular, using optical platforms, various teams have achieved non-reciprocal light propagation, enhanced sensitivity at an exceptional point, optomechanically induced transparency, and coherent perfect absorption [4], [5], [6], [7].

In optical systems, the paraxial wave equation is similar to the Schrödinger equation, which provides theoretical support for the study of PT-symmetry in optics. In addition, the refractive index of the optical materials corresponds to the potential energy term in quantum systems. The Hamiltonian PT-symmetry requirement is $V(X) = V^*(-\widehat{X})$, which is expressed in an optical system as $n_R(X) = n_R(-X)$ and $n_I(X) = -n_I(-X)$. In an odd-even time-symmetric system, the point at which multiple parameters lead to a non-Hermitian degeneracy is known as an exceptional point (EP). In the past decade, researchers have discovered several interesting phenomena near EPs [4], [8], [9]. With the maturation of waveguide technology, EPs with various structures and materials in the optical field have been constructed. Two-level system is a common scheme for building non-Hermitian platforms. For example, two evanescently coupled optical waveguides with gain and loss balanced materials ($Al_aGa_{1-a}As$ heterostructure and Cr) lead to loss-induced optical transparency. WGM optical resonator (silica) is the focus of constructing non-Hermitian system, for example, coherent perfect absorption at exceptional point with loss-only WGM resonator was achieved by tuning the distance of double ring. [5], [10] Additionally, various optical systems have been observed, such as laser absorption transitions, and single-mode lasers [11], [12], [13], [14], [15]. The system transitions from having real to complex frequencies near the EP. This transition from the exact- to broken-PT phase induces a series of complex but more exotic phenomena [14], [16]. However, the properties of EP point have not been extensively studied in the cavity made of lithium niobate, especially in combination with the electro-optical effect of lithium niobate.

Lithium niobate plays a key role in optoelectronic research. With the gradual maturation of on-chip integration technology, lithium niobate is favored for its excellent optical properties in electro-optic modulators, optical switches, filters, and other applications [17]. Furthermore, lithium niobate has large electro-optic coefficients. Essentially, the real part of the refractive index of the material can be easily altered by exerting horizontal electric fields of different intensities. In particular, the imaginary part of the refractive index can be equivalent by the light amplification process of Erbium-doped lithium niobate. [18], [19], [20]. Phang et al. reported skewness due to dispersion and frequency

Manuscript received 4 August 2022; revised 28 August 2022; accepted 31 August 2022. Date of publication 5 September 2022; date of current version 16 September 2022. This work was supported in part by the National Natural Science Foundation of China under Grants 61775084 and 62075088, in part by the NSAF under Grant U2030103, in part by the Natural Science Foundation of Guangdong Province under Grants 2020A1515010791 and 2021A0505030036, in part by the Open Fund of Guangdong Provincial Key Laboratory of Information Photonics Technology of Guangdong University of Technology under Grant GKPT20-03, and in part by the Fundamental Research Funds for the Central Universities under Grants 21622107 and 21622403. *(Corresponding authors: Huihui Lu; Heyuan Guan.)*

Xianpeng Lv, Qijing Lin, Heyuan Guan, and Huihui Lu are with the Guangdong Provincial Key Laboratory of Optical Fiber Sensing and Communications, Department of Optoelectronic Engineering, Jinan University, Guangzhou 510632, China (e-mail: 2020lxp@stu2020.jnu.edu.cn; agglll@stu2020.jnu.edu.cn; ttguanheyuan@jnu.edu.cn; thuihuilu@jnu.edu.cn).

Wentao Qiu is with the Key Laboratory of Optoelectronic Information and Sensing Technologies of Guangdong Higher Education Institutes, Jinan University, Guangzhou 510632, China (e-mail: qiuwentao@jnu.edu.cn).

Digital Object Identifier 10.1109/JPHOT.2022.3204366

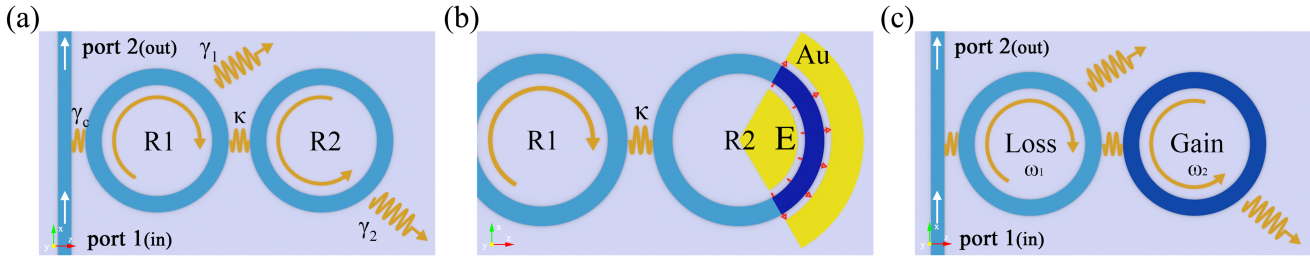

Fig. 1. (a) Schematic diagram of double ring resonator with LN. (b) The electric field covers the area. (c) Gain material area (marked in dark blue).

misalignment during eigenfrequency splitting of PT symmetric resonators [21]. However, there is no systematic study on the effect of dispersion or the real part of the refractive index on the system response and the change of the applied electric field. We take advantage of the excellent electro-optic effect of lithium niobate, we can continuously change the refractive index by adjusting the intensity of the applied electric field, which can study the system response to the the electric field distribution.

To this end, the construction of an EP based on a resonator is a common solution [12], [14], [22], [23], [24], [25]. Based on the above-mentioned construction method, we used a double-ring resonator with a direct-coupling waveguide in this study. A straight waveguide was used as the receiving input and output. In the simulation, based on the electro-optic coefficient of lithium niobate, we calculated the change in real part of the refractive index through the actual electric field size using a theoretical method. The change in refractive index relies on an adjustable electric field between the metal electrodes, which integrate on one side of one of the ring resonators. In addition, we use erbium-doped lithium niobate in the excited state to simulate the gain. It provided a gain over a narrow wavelength range; despite the absence of pumping, the effect of the imaginary part closely fit the theoretical calculation. At the same time, we study the influence of different states of the zero and pole on the transmission spectrum of the system, and observe the evolution of the transmission spectrum: from single peak to double peak, and further to three peaks (two absorption peaks and one gain peak). Furthermore, we demonstrate the different electric-field distribution can electro-optically and accordingly change the transmission spectrum. In future, this research can be potentially applied to several fields, such as tunable and active integrated optical devices and photodetection. In particular, the tunable system has the characteristics of fast response and high tuning efficiency of lithium niobate material. Compared with thermal tuning systems, electro-optic tuning systems have its advantages in flexibility and response time.

II. Temporal Coupled-Mode Theory

A simple two-level system can be described by constructing its Hamiltonian. We constructed a non-Hermitian system comprising two lithium niobate ring resonators, as shown in Fig. 1. The thickness of the lithium niobate waveguide is 350 nm, the width is 740 nm, and the inner diameter of the ring is 4.63 μm. Herein, the resonant frequency of the resonator is $\omega_{1,2}$, loss coefficient is $\gamma_{1,2}$, coupling coefficient between the straight waveguide on one side and the system is γ_c, and coupling coefficient between the rings is κ. The effective Hamiltonian of the system can be obtained as follows.

$$H_e = \begin{pmatrix} \omega_1 - i\frac{\gamma_1+\gamma_c}{2} & \kappa \\ \kappa & \omega_2 - i\frac{\gamma_2+\gamma_c}{2} \end{pmatrix} \tag{1}$$

To derive the S-matrix of the system based on temporal coupled-mode theory [26], the S-matrix of the system can be described as follows, and we define $\Delta_{1,2} = \delta_{1,2} + i\frac{\gamma_{1,2}+\gamma_c}{2}$ and $\delta_{1,2} = \omega - \omega_{1,2}$. M in the equation represents the transmission matrix of the system in the non-resonant state.

$$S = M \begin{pmatrix} -i\frac{\gamma_c\kappa}{\Delta_1\Delta_2-\kappa^2} & 1 - i\frac{\gamma_c\Delta_2}{\Delta_1\Delta_2-\kappa^2} \\ 1 - i\frac{\gamma_c\Delta_1}{\Delta_1\Delta_2-\kappa^2} & -i\frac{\gamma_c\kappa}{\Delta_1\Delta_2-\kappa^2} \end{pmatrix} \tag{2}$$

To obtain the transmission spectrum of the system, we analyzed the eigenvalues of the effective Hamiltonian. The eigenvalue of the system is obtained by solving the following quadratic equation.

$$\omega_{\lambda\pm} = \frac{\omega_1+\omega_2}{2} \pm \sqrt{\zeta_1} - i\frac{\gamma_1+\gamma_2+2\gamma_c}{4} \tag{3}$$

Where $\zeta_1 = (\frac{\omega_1-\omega_2}{2} + i\frac{\gamma_2-\gamma_1}{4})^2 + \kappa^2$. This eigenvalue is a pole of S. It can be observed that the eigenvalue consists of two parts. The real part of the eigenvalue without considering the zeta term depends on the mean value of the resonant frequency of the resonant cavity. Whereas, the imaginary part comprises the loss coefficients of the system; γ_c and γ_c can be regarded as the loss of the system. When ζ is considered, the real and imaginary parts of the eigenvalue degenerate and separate. At the critical point of this phenomenon, we regarded eigenvalue of the system it as the EP point of the system pole. For the zero point, we obtain the zero corresponding to the eigenvalue as follows.

$$\omega_{z\pm} = \frac{\omega_1+\omega_2}{2} \pm \sqrt{\zeta_2} + i\frac{2\gamma_c-\gamma_1-\gamma_2}{4} \tag{4}$$

Where $\zeta_2 = (\frac{\omega_1-\omega_2}{2} + i\frac{\gamma_2-\gamma_1}{4})^2 + \kappa^2$. From the calculations presented above, we obtained two poles and two zeros of the system. Next, we obtained the function and image of the system transmission spectrum by analyzing the changes in the zeros and poles in different parameter spaces.

According to the S matrix, we can obtain the transmittance of port 2 when port 1 is excited from S_{21}, and we define $\gamma_{d1,s1} =$

$\gamma_1 \pm \gamma_c$ and $\gamma_{s2} = \gamma_2 + \gamma_c$:

$$|t_{21}|^2 = M^2 \frac{\left(\delta_1\delta_2 - \frac{\gamma_{d1}\gamma_{s2}}{4} - \kappa^2\right)^2 + \left(\delta_1\frac{\gamma_{s2}}{2} + \delta_2\frac{\gamma_{d1}}{2}\right)^2}{\left(\delta_1\delta_2 - \frac{\gamma_{s1}\gamma_{s2}}{4} - \kappa^2\right)^2 + \left(\delta_1\frac{\gamma_{s2}}{2} + \delta_2\frac{\gamma_{s1}}{2}\right)^2} \quad (5)$$

III. Effect of Electric Field

To avoid the influence of different resonance frequencies, we introduce a straight waveguide as shown in Fig. 1(a), we must adjust the resonant frequency of the two resonators such that they are consistent, which is achieved by fine-tuning the outer radius of the second ring; essentially, $\omega_1 = \omega_2$. When we adjust the distance between the two rings, a variation of κ can be correspondingly obtained. The coupling coefficient is reduced by increasing the distance between the rings, and degeneracy of zeros and poles occurs simultaneously when $4\kappa = |\gamma_1 - \gamma_2|$. [5]

As shown in Fig. 1(b), a sector electrode with an angle of 120° was placed in the right resonator cavity. The simulation is carried out with the FDTD (Lumerical Inc.) software. In the simulation, we approximated the electric field distribution of the sector as a uniform electric field along the Z-axis. To observe change in the transmission spectrum, we selected the state in which the degeneracy of zeros and poles did not occur as the reference state. In the simulation process, because the effect of the approximate electric field on the lithium niobate material was along the Z-axis direction, due to the anisotropy of lithium niobate [18], the ϵ_{33} of the lithium niobate material was affected by the applied electric field with the properties of anisotropy; additionally, the electric field intensity corresponding to the refractive index change was calculated using the electro-optic coefficient. Where $n = n_e = 2.139$ and $\gamma_{33} = 33\ pm/V$.

$$\Delta n = -\frac{1}{2} \times n^3 \times \gamma_{33} \times E_z \quad (6)$$

During simulation, we limited the refractive index variation of the material from -0.015 to 0.015. The variation range of the transverse electric field was from $-1.13 \times 10^8\ V/m$ to $1.13 \times 10^8\ V/m$, as obtained by (6). Next, we traversed the values in this range with a step size of 0.00375, which is $2.27 \times 10^7\ V/m$. Simultaneously, we fit the transmission spectrum obtained by the simulation through (5) and obtained the transmission spectrum, as shown in Fig. 2(a),(b), through lateral comparison. By comparing the projected spectra of different electric fields, we found that the characteristic peak in the transmission spectrum shifted with the electric field strength and direction, with a maximum frequency shift of 149 GHz. Furthermore, at $E = |1.13 \times 10^8|\ V/m$, the contrast of the two characteristic peaks reached 0.43 ($Contrast = \frac{|I_1 - I_2|}{I_1 + I_2}$, where $I_{1,2}$ refers to the transmitted light intensity at the two peaks). Fig. 2(c),(d) demonstrate that the tunable system suppresses the resonance detuning between the resonators by controlling the dispersion. The eigenfrequency degenerates when the detuning is zero, and the tunable system exhibits the ability to control the EP.

The electric-field diagram in Fig. 3 shows the state of the two characteristic peaks under the influence of the maximum electric field. As illustrated in Fig. 3(a)–(d), it is observed that

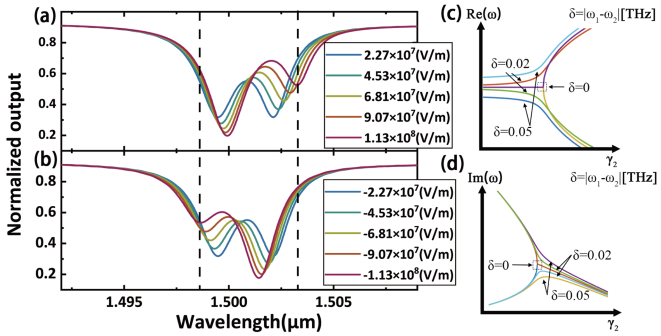

Fig. 2. (a) Transmitted spectra of the positive electric field. (b) Transmitted spectrum of the negative electric field. (c) Dispersion variation induces the disappearance of the EP (the real part). (d) Dispersion variation induces the disappearance of EP (the imaginary part).

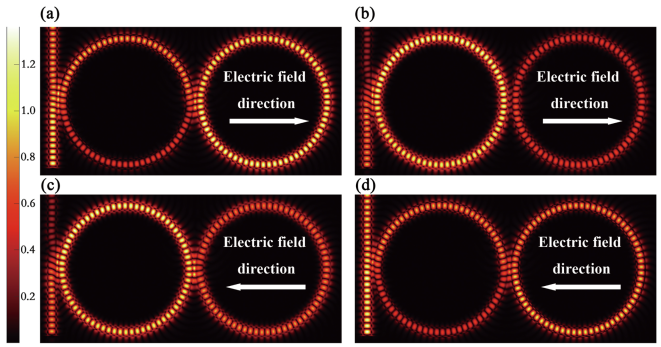

Fig. 3. The electric field distribution at the characteristic peak from right (a) to left (b) under the forward electric field, respectively. the electric field distribution at the characteristic peak from right (c) to left (d) under the backward electric field, respectively.

the energy distributions of the left and right characteristic peaks are exchanged, and the energy distribution states in the two rings can be changed by changing the direction of the electric field, respectively.

EP emphasizes the high symmetry of the refractive index of the material in the spatial domain. Based on the ability of lithium niobate to change the dispersion of the waveguide, the symmetric structure that depends on the material and structure can be transformed into a symmetric structure based on electric field control. Different from the strict PT symmetry requirement, the local tuning of the resonator causes the PT symmetry to be broken locally (The refractive index of lithium niobate with applied electric field can be electro-optic changed), but the whole system still exhibits the characteristics of PT symmetry (EP appearance). This "quasi-symmetry" offers the possibility of constructing EPs for more complex structures.

IV. Influence Under Gain Material

Considering a general case, the introduction of gain material into a system may result in a negative loss coefficient for some parts of the system. However, without the introduction of gain, the poles of the system tend to have complex numbers. Optical gain $\gamma_{1,2}$ is provided through stimulated radiation using erbium doped lithium niobate material [21], [27], [28]. In recent years,

TABLE I
LIST OF PARAMETERS AFTER FITTING THE TRANSMISSION SPECTRUM USING (5) UNDER DIFFERENT GAIN INTENSITIES

Data index	$\omega_1(THz)$	$\omega_2(THz)$	$\gamma_1(THz)$	$\gamma_2(THz)$	$\kappa(THz)$
D1/fitting 1	199.791	199.796	0.201	0.184	0.073
D2/fitting 2	199.790	199.796	0.205	0.052	0.068
D3/fitting 3	199.791	199.794	0.207	0.001	0.066
D4/fitting 4	199.788	199.792	0.211	-0.068	0.064
D5/fitting 5	199.790	199.795	0.210	-0.097	0.064
D6/fitting 6	199.788	199.796	0.213	-0.091	0.065
D7/fitting 7	199.788	199.795	0.212	-0.113	0.067

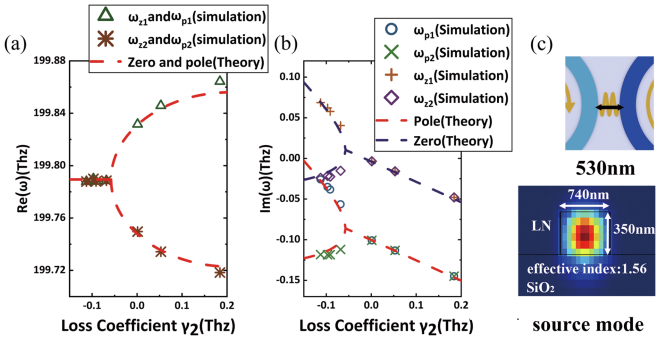

Fig. 4. (a) Distribution of poles and zeros on the real axis for different gains. (b) Distribution of poles and zeros on the imaginary axis at different gains. (c) Ring distance and light source settings.

lithium niobate materials that realize optical amplification by erbium doping have been experimentally proved their feasibility. In the simulation process, "Four-level material" is used to approximate doped lithium niobate with optical amplification in the 1500 nm band. [29] As shown in Fig. 1(c), the resonator on the right is set to gain lithium niobate material. Moreover, the initial state of the doped lithium niobate material is an excited state. The generation of the excited state can be realized by simulating the pump source or directly setting the initial state as the excited state.

Here, we derive the transmission map of port 2, as shown in Fig. 1(a) and (c), through simulation and equation fitting. According to the S-matrix. To avoid the deviation of the resonant frequency of the left resonant cavity caused by the introduction of a straight waveguide, the resonant frequencies of the two cavities were made consistent by slightly adjusting the diameter of the right resonant cavity during the simulation. We considered the coupling strength of $\kappa \approx 0.065$ as the standard state of the simulation. In the gain material simulation, the concentration of free electrons doped with lithium niobate as a carrier was increased from 0.006 mol/m^3 to 0.012 mol/m^3. With the increase in the doping concentration, there was a decrease in the value of γ_2.

Based on the change in the gain or loss coefficient, (5) was used to fit the simulation experimental data to obtain the fitting values of the parameters in the equation. The specific fitting parameters are listed in Table I.

A series of such fitting parameters was averaged to obtain the average number of parameters. Subsequently, the function with γ_2 as the independent variable was obtained from the average number of parameters, as shown in Fig. 4. For such parameter

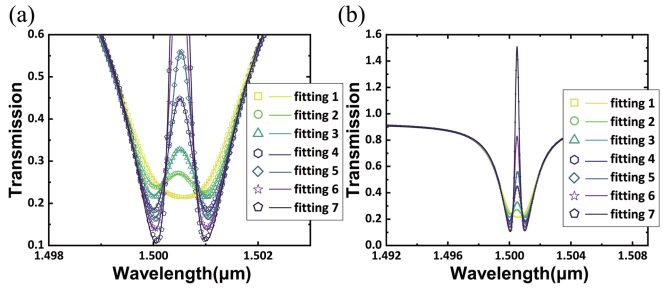

Fig. 5. (a) Transmitted spectra at different gains after fitting according to (5). (b) A local enlargement of characteristics of transmission spectra.

changes, the overall loss coefficient of resonator R2 produced a phase change of approximately -0.06. The EP of the zero and pole was approximately zero. In the case of a single channel, the functions of the pole and zero with respect to γ_2 were consistent in the real part, whereas the imaginary part differed by a constant. The zeros met when γ_2 was negative and separated at -0.06. Contrastingly, the poles met when γ_2 was positive. When the absolute value of γ_2 was close to 0.06, the imaginary part of the zero point disappeared, the zero point moved to the real axis, and two zero points to the right of $\gamma_2 = -0.06$ moved to the real axis simultaneously. For the poles, the curve in Fig. 4(b) shows that when the gain was close to -0.15, the imaginary part of one of the poles disappeared, the pole moved to the real axis, and transmittance became infinite near the pole. The EP point can be obtained from the critical point where the eigenfrequency splits occur in the graph. Fig. 4(c) shows the distance between rings and light source settings in the simulation.

We used (5) to obtain the transmittance of port 2 in the CW mode, and subsequently obtained the seven sets of curves, as shown in Fig. 5. The curve in the figure shows the change in the transmission spectrum under the combined action of the different zeros and poles. It is noteworthy that in the case of no gain, the transmission spectrum was a single valley owing to the low coupling coefficient of the two resonators. During the gradual application of gain intensity, a peak appeared at the bottom of the valley and increased as the gain increased. When the gain term $\gamma_2 \approx -0.1$, the transmittance at the resonance was one. By further increasing the gain, the transmittance of the center frequency broke through one, thereby indicating that the energy was enhanced while the nearby frequencies remained in the absorption state. The continuous enhancement of the gain resulted in the narrowing of the line width at the center frequency. In an ideal case, the system diverges because the pole was close to the real axis and the center frequency was close to the pole. Furthermore, the simulation results revealed that the absorption coefficients at the valley bottoms on both sides of the center frequency were different.

V. CONCLUSION

We introduced a single-channel dual-resonator system by varying several parameters to observe the behavior mode of the system near the EP point. First, we changed the refractive index of one of the rings with an electric field of 1.13×10^8 V/m.

This resulted in a double transmission-valley difference from 0 to 0.33, and a maximum frequency shift of 149 GHz. Next, we obtained the degeneracy and degradation of the zeros and poles of the system scattering matrix caused by $\gamma_2 = -0.06$ by equivalently changing one of the imaginary parts of the ring refractive index. This study provides new properties of active open systems for on-chip integrated optics based on lithium niobate materials, which is expected to further expand the application prospects of lithium niobate materials.

REFERENCES

[1] L. Feng, R. El-Ganainy, and L. Ge, "Non-Hermitian photonics based on parity-time symmetry," *Nature Photon.*, vol. 11, no. 12, pp. 752–762, 2017.

[2] R. El-Ganainy, K. G. Makris, M. Khajavikhan, Z. H. Musslimani, S. Rotter, and D. N. Christodoulides, "Non-Hermitian physics and PT symmetry," *Nature Phys.*, vol. 14, no. 1, pp. 11–19, 2018.

[3] C. M. Bender, "Making sense of non-Hermitian Hamiltonians," *Rep. Prog. Phys.*, vol. 70, no. 6, pp. 947–1018, 2007.

[4] S. B. Wang, B. Hou, W. X. Lu, Y. T. Chen, Z. Q. Zhang, and C. T. Chan, "Arbitrary order exceptional point induced by photonic spin-orbit interaction in coupled resonators," *Nature Commun.*, vol. 10, 2019, Art. no. 832.

[5] C. Q. Wang, W. R. Sweeney, A. D. Stone, and L. Yang, "Coherent perfect absorption at an exceptional point," *Science*, vol. 373, no. 6560, pp. 1261–1265, 2021.

[6] C. E. Rüter, K. G. Makris, R. El-Ganainy, D. N. Christodoulides, M. Segev, and D. Kip, "Observation of parity–time symmetry in optics," *Nature Phys.*, vol. 6, no. 3, pp. 192–195, 2010.

[7] H. Jing et al., "Optomechanically-induced transparency in parity-time-symmetric microresonators," *Sci. Rep.*, vol. 5, 2015, Art. no. 9663.

[8] M. A. Miri and A. Alu, "Exceptional points in optics and photonics," *Science*, vol. 363, no. 6422, 2019, Art. no. eaar7709.

[9] W. D. Heiss, "Exceptional points of non-Hermitian operators," *J. Phys. A: Math. Gen.*, vol. 37, no. 6, pp. 2455–2464, 2004.

[10] A. Guo et al., "Observation of PT-symmetry breaking in complex optical potentials," *Phys. Rev. Lett.*, vol. 103, no. 9, 2009, Art. no. 093902.

[11] W. R. Sweeney, C. W. Hsu, S. Rotter, and A. D. Stone, "Perfectly absorbing exceptional points and chiral absorbers," *Phys. Rev. Lett.*, vol. 122, no. 9, 2019, Art. no. 093901.

[12] J. Zhang et al., "A phonon laser operating at an exceptional point," *Nature Photon.*, vol. 12, no. 8, pp. 479–484, 2018.

[13] M. Brandstetter et al., "Reversing the pump dependence of a laser at an exceptional point," *Nature Commun.*, vol. 5, no. 1, 2014, Art. no. 4034.

[14] L. Feng, Z. J. Wong, R. M. Ma, Y. Wang, and X. Zhang, "Single-mode laser by parity-time symmetry breaking," *Science*, vol. 346, no. 6212, pp. 972–975, 2014.

[15] W. J. Wan, Y. D. Chong, L. Ge, H. Noh, A. D. Stone, and H. Cao, "Time-reversed lasing and interferometric control of absorption," *Science*, vol. 331, no. 6019, pp. 889–892, 2011.

[16] Y. D. Chong, L. Ge, and A. D. Stone, "PT-symmetry breaking and laser-absorber modes in optical scattering systems," *Phys. Rev. Lett.*, vol. 106, no. 9, 2011, Art. no. 093902.

[17] C. Wang et al., "Integrated lithium niobate electro-optic modulators operating at CMOS-compatible voltages," *Nature*, vol. 562, no. 7725, pp. 101–104, 2018.

[18] R. S. Weis and T. K. Gaylord, "Lithium niobate: Summary of physical properties and crystal structure," *Appl. Phys. A*, vol. 37, no. 4, pp. 191–203, 1985.

[19] K. Liu, J. H. Shi, and X. F. Chen, "Electro-optical flat-top bandpass Solc-type filter in periodically poled lithium niobate," *Opt. Lett.*, vol. 34, no. 7, pp. 1051–1053, 2009.

[20] Y. Wang et al., "Electro-optic beam deflection based on a lithium niobate waveguide with microstructured serrated electrodes," *Opt. Lett.*, vol. 41, no. 20, pp. 4739–4742, 2016.

[21] B. Peng et al., "Parity–time-symmetric whispering-gallery microcavities," *Nature Phys.*, vol. 10, no. 5, pp. 394–398, 2014.

[22] L. Chang et al., "Parity-time symmetry and variable optical isolation in active-passive-coupled microresonators," *Nature Photon.*, vol. 8, no. 7, pp. 524–529, 2014.

[23] M. Liertzer, L. Ge, A. Cerjan, A. D. Stone, H. E. Tureci, and S. Rotter, "Pump-induced exceptional points in lasers," *Phys. Rev. Lett.*, vol. 108, no. 17, 2012, Art. no. 173901.

[24] F. X. Zhang, Y. M. Feng, X. F. Chen, L. Ge, and W. J. Wan, "Synthetic anti-PT symmetry in a single microcavity," *Phys. Rev. Lett.*, vol. 124, no. 5, 2020, Art. no. 053901.

[25] R. El-Ganainy, K. G. Makris, D. N. Christodoulides, and Z. H. Musslimani, "Theory of coupled optical PT-symmetric structures," *Opt. Lett.*, vol. 32, no. 17, pp. 2632–2634, 2007.

[26] H. A. Haus, *Waves and Fields in Optoelectronics*. Hoboken, NJ, USA: Prentice-Hall, 1984.

[27] Q. Luo et al., "On-chip erbium-doped lithium niobate microring lasers," *Opt. Lett.*, vol. 46, no. 13, pp. 3275–3278, 2021.

[28] L. Chang et al., "Parity–time symmetry and variable optical isolation in active–passive-coupled microresonators," *Nature Photon.*, vol. 8, no. 7, pp. 524–529, 2014.

[29] S.-H. Chang and A. Taflove, "Finite-difference time-domain model of lasing action in a four-level two-electron atomic system," *Opt. Exp.*, vol. 12, no. 16, pp. 3827–3833, 2004.